J Biomol NMR (2013) 57:103–116
DOI 10.1007/s10858-013-9770-6

ARTICLE

Structural and dynamical characterization of the Miz-1 zinc fingers 5–8 by solution-state NMR

David Bernard · Mikaël Bédard · Josée Bilodeau · Pierre Lavigne

Received: 12 June 2013 / Accepted: 6 August 2013 / Published online: 24 August 2013

Abstract Myc-interacting zinc finger protein-1 (Miz-1) is a BTB/POZ transcription factor that activates the transcription of cytostatic genes, such as $p15^{INK4B}$ or $p21^{CIP1}$. The C-terminus of Miz-1 contains 13 consensus C_2H_2 zinc finger domains (ZF). ZFs 1–4 have been shown to interact with SMAD3/4, while the remaining ZFs are expected to bind the promoters of target genes. We have noted unusual features in ZF 5 and the linker between ZFs 5 and 6. Indeed, a glutamate is found instead of the conserved basic residue two positions before the second zinc-coordinating histidine on the ZF 5 helix, and the linker sequence is DTDKE in place of the classical TGEKP sequence. In a canonical ββα fold, such unusual primary structure elements should cause severe electrostatic repulsions. In this context, we have characterized the structure and the dynamics of a Miz-1 construct comprising ZFs 5–8 (Miz 5–8) by solution-state NMR. Whilst ZFs 5, 7 and 8 were shown to adopt the classical ββα fold for C_2H_2 ZFs, the number of long-range NOEs was insufficient to define a classical fold for ZF 6. We show by using ^{15}N-relaxation dispersion experiments that this lack of NOEs is due to the presence of extensive motions on the μs–ms timescale. Since this negatively charged region would have to be located near the phosphodiester backbone in a DNA complex, we propose that in addition to promoting conformational searches, it could serve as a hinge region to keep ZFs 1–4 away from DNA.

Keywords Miz-1 · Solution structure · Zinc fingers · Protein dynamics · Conformational exchange

Abbreviations

CD	Circular dichroism
Miz 5-8	Miz-1 zinc fingers 5–8
NMR	Nuclear magnetic resonance spectroscopy
Water-TFA	0.1 % trifluoroacetic acid in water
ZF	Zinc finger

Introduction

Myc-interacting zinc finger protein-1 (Miz-1) is a member of the BTB/POZ transcription factor family. It is 803-amino-acid long and weighs 93 kDa. Like all members of the family, it possesses a BTB/POZ protein interaction domain at its N-terminus and a number (thirteen) of putative zinc finger domains (ZF) in its C-terminus. The crystal structure of the Miz-1 BTB/POZ has been solved (Stead et al. 2007; Stogios et al. 2010). Twelve of the Miz-1 ZFs are consecutive, and the thirteenth is remote from the twelfth by a sequence that has been identified as a Myc-interacting domain. Another such domain exists between the BTB/POZ domain and the first ZF (Peukert et al. 1997).

Electronic supplementary material The online version of this article (doi:10.1007/s10858-013-9770-6) contains supplementary material, which is available to authorized users.

D. Bernard · M. Bédard · J. Bilodeau · P. Lavigne (✉)
Département de Biochimie, Faculté de Médecine et des Sciences de la Santé, Institut de Pharmacologie de Sherbrooke, Université de Sherbrooke, 3001, 12e avenue Nord, Sherbrooke, QC J1H 5N4, Canada
e-mail: pierre.lavigne@usherbrooke.ca

D. Bernard · M. Bédard · J. Bilodeau · P. Lavigne
Regroupement Stratégique sur la Fonction, la Structure et l'Ingénierie des Protéines (PROTEO), Québec, Canada

D. Bernard · M. Bédard · J. Bilodeau · P. Lavigne
Groupe de Recherche Axé sur la Structure des Protéines (GRASP), Montréal, Canada

Miz-1, which can be activated through the TGF-β pathway, activates the transcription of various cytostatic genes, such as $p15^{INK4B}$ and $p21^{CIP1}$. Miz-1 and Sp1 both bind the core promoter of those genes (Bowen 2003) and nucleophosmin binds to the BTB/POZ domain of Miz-1 (Wanzel et al. 2008). This allows histone acetyltransferase p300 to be recruited, which activates transcription. When c-Myc binds Miz-1 (as a c-Myc/Max heterodimer), the recruitment of p300 becomes impossible and the complex represses transcription (Seoane et al. 2001; Staller et al. 2001).

It is thought that a subset of the thirteen putative C_2H_2 ZFs is responsible for the DNA-binding activity associated with the Miz-1 protein. Indeed, ZFs are very common DNA-binding motifs. In fact, it is the most common motif found in the human genome (Razin et al. 2012; Wolfe et al. 2000). C_2H_2 ZFs are ~30-amino-acid long with the consensus sequence F/Y-X-C-X_{2-4}-C-X_3-F-X_5-L-X_2-H-X_3-H-X_5, and they usually adopt a ββα conformation (Berg 1988). This conformation is held in place by the two cysteines and the two histidines, which coordinate a Zn^{2+} ion, as well as three conserved large hydrophobic amino acids. This makes the N-terminus of the α helix protrude, and allows it to enter the major groove of the DNA. In a canonical ZF, four residues will contact the DNA bases, allowing recognition of a particular sequence. Residues situated at positions—1, 3 and 6 relative to the first residue of the helix usually contact consecutive bases on one strand, and the residue in position 2 will contact one base on the other strand. This last base is in fact the complementary base to the one contacted by the residue in position 6 of the preceding ZF. All four of these contacts can be base-specific. ZFs usually bind DNA by groups of three, allowing specific recognition of sequences 10 bp long [reviewed in Wolfe et al. (2000)].

ZFs are typically separated by a conserved linker with the consensus sequence TGEKP. Interestingly, the lysine in the linker is often involved in non-specific salt bridges with phosphate groups when ZFs are bound to DNA. Moreover, a salt bridge between the conserved glutamate and a conserved basic side chain (arginine or lysine) in the preceding helix has been demonstrated to be important in the modulation of inter-ZF movements. Indeed, when a salt bridge is not possible, the inter-ZF movements are amplified and this is thought to be important for the mechanism of recognition of specific DNA sequences by polydactyl ZF proteins (Zandarashvili et al. 2012).

Recent bioinformatics studies have demonstrated that the residues at positions—1, 2, 3, 5 and 6 in the α-helix are the only residues in ZFs displaying selective pressure during evolution (Emerson and Thomas 2009). While this could be interpreted as an evolutive pressure to bind diverse DNA sequences, it could also mean that they have evolved for other functions, such as protein binding. In fact, it is becoming increasingly recognized that ZFs are also important actors in protein–protein interactions (Brayer and Segal 2008). In accordance with this growing concept, the first 4 ZFs of Miz-1 have been shown to interact with the MH1 domain of SMAD3 and 4 (Seoane et al. 2001).

While the binding of Miz-1 has been narrowed down to two distant sites at the promoters of $p15^{INK4B}$ (−155/−140, −1/13) and $p21^{CIP1}$ (−105/−81, −46/−32) (Seoane et al. 2002), the exact ZFs involved have yet to be identified. Interestingly, application of the most recent bioinformatics programs fails to generate a consistent prediction as to which ZF subset (equal to or larger than 3) have the highest probability of binding the identified sequences on the $p15^{INK4B}$ and $p21^{CIP1}$ promoters.

In this context, we have undertaken a structural and dynamical characterization of the Miz-1 ZFs in absence of DNA with determination of the NMR structure of ZF domains 8–10 (Bédard et al. 2012). The three ZFs were demonstrated to adopt the typical ββα fold. In accordance with previous reports (Hyre and Klevit 1998; Potter 2005; Zandarashvili et al. 2012), the two canonical linkers (TGEKP) were shown to be the most flexible regions on the ps–ns timescale without, however, being totally unfolded. In the present study, we extend our structural and dynamical characterization of Miz-1 ZFs with a construct composed of ZFs 5–8 (henceforth referred to as Miz 5–8).

Whereas ZF 5, ZF 7 and ZF 8 are shown to adopt a stable ββα fold, the structure of ZF 6 appears to undergo a slow (μs–ms) conformational change. Moreover, we also note the presence of extensive conformational exchange in the μs–ms timescale at the interface between the helices of ZF 5, ZF 6 and ZF 7 and the contiguous linkers. Although such movements have been noted between ZF 1 and ZF 2 of Egr-1 (Zif268) (Zandarashvili et al. 2012), those observed in the Miz 5–8 construct appear exacerbated. In fact, the movements in the Egr-1 construct have been attributed to the absence of the conserved E in the linker (TG**Q**KP) between ZF 1 and ZF 2. Interestingly, two out of three linkers in the Miz 5–8 construct have more peculiar sequences; DTDKE and IADGP. As described in detail, electrostatic repulsions located at the interface between the helix of ZF 5 and the contiguous linker are most likely responsible for the local unfolding in ZF 6. While a role for such unusual slow conformational exchange in the DNA and/or protein binding remains to be determined, we show by homology modeling that DNA binding by ZF 5 and 6 is highly unlikely. Indeed, because of the sequence of the linker between ZF 5 and 6, intramolecular and intermolecular electrostatic repulsion in a canonical DNA-bound configuration would prevent DNA binding. We propose that this peculiar sequence and resultant dynamical behavior might be important for Miz-1 function by promoting the availability of ZF 1–4 to engage in protein–protein interaction with SMAD3/4.

Materials and methods

Preparation of the Miz 5–8 construct

The cDNA fragment of ZFs 5–8 of Miz-1 (residues 416–526, Miz 5–8, see primary structure in Fig. 1a) was generated by PCR from the complete cDNA of Miz-1 using primers F (5′-CAT ATG AAG CCC TAC CAG TGC GAC TAC TGC GGC CG-3′) and R (5′-GGA TCC CTA ACC TGT GTG AAT GCG GAC GTG CCG CTG-3′). The PCR product was inserted into a pDrive (Qiagen) vector prior to a digestion by NdeI and BamHI. The digested product was inserted into a pET-3a (Novagen) plasmid by the same restriction sites and the construct transformed in BL21 star (DE3*) one shot competent cells (Invitrogen). Bacteria were grown in LB or in M9 broth (supplemented with 10 μM $FeSO_{4-}$ and 100 μM $CaCl_2$) containing $^{15}NH_4Cl$ and ^{13}C-glucose to an O.D. of 0.6 at 600 nm; they were induced with 1 mM IPTG and 100 μM $ZnCl_2$ for 21 h at 30 °C and they were harvested by centrifugation. The cell pellet was resuspended in lysis buffer (800 mM NaCl, 50 mM KH_2PO_4, 100 mM DTT) and frozen at −80 °C for at least 2 h prior to thawing in hot water. The lysate was treated with 50 mg/ml of DNAseI for 1 h at room temperature and centrifugated at 30,000 RCF for 30 min. The supernatant was diluted by a factor 2 with Tris–HCl pH 7.6 and purified by FPLC with a HiTrap SP HP column (GE Healthcare) using buffer A (50 mM sodium acetate, pH 5.00). After eluting impurities using a mix of buffer A containing 14 % of buffer B (50 mM sodium acetate, 3 M NaCl, pH 5.00), Miz 5–8 was eluted using a gradient of buffer B. Fractions containing Miz 5–8 were pooled and desalted on FPLC using HiTrap Desalting columns (GE Healthcare) with water containing 0.1 % trifluoroacetic acid (water-TFA) as elution buffer. The sample was then concentrated using ultracentrifugation (Amicon Ultra 3 K, Millipore). Finally, the protein was purified by reverse-phase HPLC with a Discovery BIO Wide Pore C18 column (Supelco) preconditioned with water-TFA and eluted using a gradient of acetonitrile. Fractions containing Miz 5–8 were lyophilized and resuspended in water-TFA so that cysteines remain in reduced form.

CD spectropolarimetry

CD measurements were performed with a Jasco J-810 spectropolarimeter equipped with a Jasco Peltier-type thermostat. The CD spectra were recorded at 20 °C with 40 μM of Miz 5–8 at different pH and Zn^{2+} concentrations in a 1 mm quartz cell. CD spectra were averaged over nine scans in order to enhance the signal-to-noise ratio by a factor 3. They were recorded between 190 and 250 nm with a wavelength step of 0.2 nm and smoothed using Spectra Manager (JASCO Corporation). Data was converted from CD signal to mean residue ellipticity using Eq. 1, where δ is the ellipticity in degrees, MRW is the mean residue weight, c is the concentration of the sample (g ml^{-1}) and l is the path length (cm).

$$[\Theta] = \frac{\delta \cdot MRW}{10 \cdot c \cdot l} \quad (1)$$

NMR spectroscopy

All NMR experiments were performed at 25 °C on a Varian (Agilent) Unity INOVA operating at ^{1}H frequency of 600 MHz and equipped with an indirect detection H/C/N room temperature probe and Z-axis pulsed-field gradient capacity. After refolding the uniformly ^{13}C, ^{15}N-labeled Miz 5–8 construct, the buffer was changed to 10 mM sodium cacodylate, pH 7.0, 50 mM KCl, 2 mM TCEP, 4.4 molar equivalents $ZnCl_2$, 10 % D_2O using ultracentrifugation (Amicon Ultra 3 K, Millipore). The final concentration of the Miz 5–8 construct was 1.16 mM.

The chemical shifts of Miz 5–8 ^{1}H, ^{13}C and ^{15}N nuclei were assigned using standard multi-dimensional and heteronuclear NMR experiments: ^{1}H–^{15}N HSQC, ^{1}H–^{13}C HSQC, 3D-HNCACB, CBCA(CO)NH, HNCO, C(CO)NH, H(CCO)NH, HCCH-TOCSY and ^{13}C and ^{15}N-edited-NOESY-HSQC with mixing times of 150 ms. All pulse sequences used were taken from the Biopack repertoire and based on the work of L. E. Kay. The spectra were referenced as described in Wishart et al. (1995).

^{15}N Spin relaxation

^{15}N–T_1, T_2 and {^{1}H}–^{15}N NOE experiments were recorded using previously described pulse sequences available in the Biopack repertoire (Farrow et al. 1994). Delays of 0, 30, 60, 90, 120, 150, 250, 350, 450, 550, 650, 800 and 1,000 ms and of 0, 10, 30, 50, 70, 90, 110, 130, 150, 170, 250, 350 and 490 ms were used to obtain ^{15}N–T_1 and T_2, respectively. {^{1}H}–^{15}N NOE measurements were done by comparing HSQC spectra with and without a 6-s proton saturation.

^{15}N backbone CMPG relaxation dispersion profiles were acquired in a constant time (60 ms) and interleaved manner, using a modified version of the pulse sequence from the Biopack repertoire and based on the work of Palmer et al. (Palmer et al. 2001; Wang et al. 2001) and Kay et al. (Mulder et al. 2001b). The field strengths ($\nu_{CPMG} = 1/4\tau_{CPMG}$) used were 33.3, 66.7, 100, 133, 167, 200, 267, 333, 400, 467, 533, 600, 667, 733, 800, 867, 933 and 1,000 Hz, where $2\tau_{CPMG}$ is the delay between the centers of two consecutive refocusing pulses (Mulder et al. 2001b). Experiments with $\nu_{CPMG} = 100$, 333, 867 Hz were repeated twice to estimate the extent of the experimental error. Given that only one static field was used

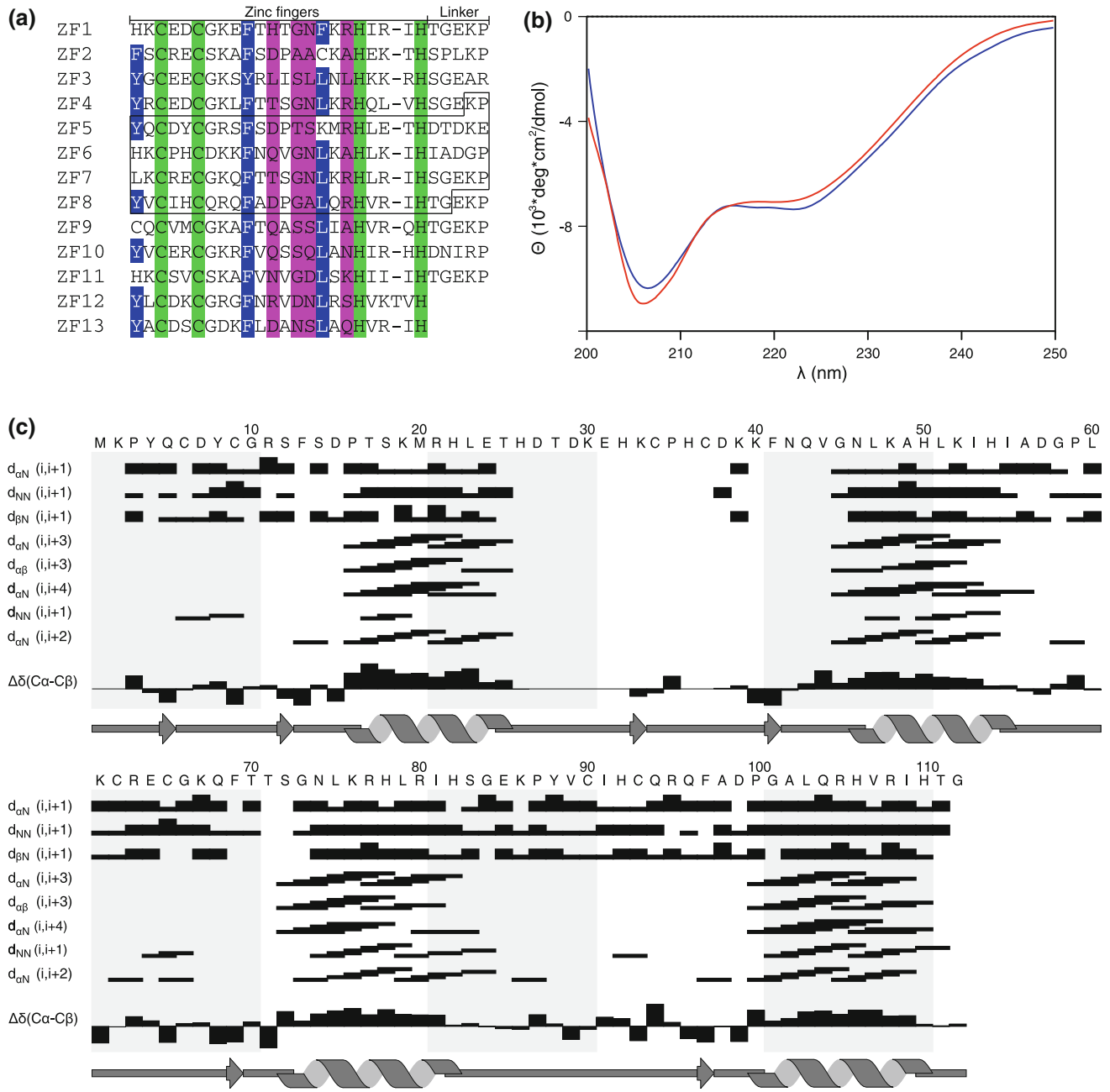

Fig. 1 Characterization of Miz 5–8 **a** Primary structure of the 13 ZF domains of Miz-1. In the complete protein, the first 12 ZFs are found within residues 306–637, and ZF 13 is within residues 717–739. Residues belonging to the Miz 5–8 fragment (416–526) are *boxed*, and are labeled residues 2–112 in this paper (residue 1 is an additional methionine). Conserved zinc-coordinating residues are highlighted in *green*, conserved hydrophobic core residues are highlighted in *blue*, and putative DNA-contacting residues are highlighted in *magenta*. **b** Far-UV CD spectrum of Miz 5–8 (*red*) and Miz 8–10 (*blue*). Results are shown in mean residue ellipticity and calculated using equation 1. **c** Sequential NOEs, chemical shift variation $\Delta\delta(C_\alpha - C_\beta)$ and secondary structure profile calculated by DANGLE for Miz 5–8

and owing to the complexity of the system, we have limited our analysis of the relaxation profiles to the estimation of R_{ex} by fitting the graphs of $R_{2,eff}$ with the $R_{2,eff}(\nu_{CPMG})$ simplified expression for a two-site exchange in the fast exchange limit (Luz and Meiboom 1963; Mulder et al. 2001a):

$$R_2(\nu_{CPMG}) = R_{2,eff}(\nu_{CPMG} \rightarrow \infty) + R_{ex}\left(1 - \frac{4\nu_{CPMG}}{k_{ex}}\tanh\left(\frac{k_{ex}}{4\nu_{CPMG}}\right)\right) \quad (2)$$

Where

$$R_{ex} = \frac{P_A P_B \Delta\omega^2}{K_{ex}} \quad (3)$$

where the data were plotted using:

$$R_{2,eff}(\nu_{CPMG}) = \frac{1}{T}\ln\frac{I(\nu_{CPMG})}{I_O} \quad (4)$$

$R_{2,eff}(\nu_{CPMG} \rightarrow \infty)$ is the effective R_2 when the frequency of refocusing reaches an infinite value, $I(\nu_{CPMG})$ and I_o are the resonance intensities of the correlations between backbone ^{15}N and $^{1}H_N$ in presence and absence of CPMG refocusing, respectively. T is the total and constant duration of the CMPG period (60 ms). P_A and P_B are the populations of the two interchanging states, $\Delta\omega$ is the difference in ^{15}N chemical shifts in both states and k_{ex}, the exchange rate, is given by $k_A + k_B$, the two rate constants of the exchange equilibrium. In the fast exchange limit ($k_{ex} >> \Delta\omega$), the populations and $\Delta\omega$ are inseparable. Nonetheless, estimation of R_{ex} values at one field is valid using this approach (Lipchock and Loria 2009).

Data processing and analysis

The NMR spectra were processed using NMRPipe (Delaglio et al. 1995) and analyzed with CcpNmr Analysis (Vranken et al. 2005). The ^{15}N–T_1 and T_2 time constants and their uncertainties were obtained by fitting the decays of the peak heights to the classical two-parameter single exponential using the least squares fitting program in CcpNmr Analysis. The relaxation dispersion profiles were fit to Eq. 2 with the program GraphPad Prism 5 in order to get R_{ex} values and their uncertainties.

Structure calculations

All NOEs were assigned manually and converted into distance restraints using CcpNmr Analysis. The program DANGLE was used to obtain φ and ψ dihedral angles on the basis of backbone and $^{13}C_\beta$ chemical shift value. Dihedral φ and ψ angles were calculated for 99 residues and they confirmed the typical ββα fold for all four ZFs, except for the first β strand of both ZFs 7 and 8. NOESY spectra revealed sequential distance restraints typical of α helices, which appear in the same regions predicted by DANGLE to fold into helical structure. Structures were calculated using the program ARIA2.2 (Rieping et al. 2007) in conjunction with CNS (Brünger et al. 1998). Calculations were first carried out without zinc atom and zinc coordination restraints. In ZF 5 and ZF 7, the conserved cysteines and histidines were positioned correctly to allow coordination of zinc. By contrast, in ZF 6, due to the lack of NOEs around the two cysteines, only the two histidines were well positioned. However, NOEs between His50 $^{1}H_{\delta 2}$ and Cys34 $^{1}H_{\beta a\ -\ b}$ could be identified, which could not be present in absence of zinc coordination. In the following calculations, a Zn^{2+} ion was added and zinc coordination distance restraints were specified to ARIA (2.3 Å for Zn^{2+}–S_γ and 2.0 Å for Zn^{2+}–$N_{\varepsilon 2}$). The 20 lowest-energy conformers out of 300 for the final iteration of the calculation were refined in water and submitted to PROCHECK_NMR (Laskowski et al. 1996) to validate the structural quality. The final structure ensembles of ZF 5 (residues 4–26), ZF 6 (residues 32–54) and ZF 7 (residues 60–83) were deposited in the protein databank (PDB) under identification codes 2m0d, 2m0e and 2m0f, respectively; and all NMR resonance assignments for Miz 5–8 was deposited in the BMRB under accession number 18806.

Results

Folding of Miz 5–8

Circular dichroism (CD) was used to monitor and optimize the folding conditions of Miz 5–8, as previously described (Bédard et al. 2012). $ZnCl_2$ was added in slight excess (4.4 molar equivalents, or 1.1 molar equivalent per finger) to the sample. The pH was then raised using NaOH until the secondary structure content was optimal as judged by the decrease in molar ellipticity between 210 and 230 nm, as well as the shifting of the minimum from 204 to 207 nm (data not shown). The optimal pH was found to be 7; a value larger than the optimal pH found for the Miz 8–10 construct (pH 6.5). We present the spectrum of Miz 5–8 shown along with that of Miz 8–10 (see Fig. 1b). As one can notice, the optimal secondary structure content of Miz 5–8 is comparable to that of Miz 8–10.

Resonance assignments and secondary structure of Miz 5–8

The dataset recorded (see materials and methods) allowed for the assignment of 86.4 % of the backbone $^{15}N_H$, 91.3 % of the $^{1}H_N$, 85.5 % of the $^{13}C'$, 93.6 % of the $^{13}C_\alpha$, 85.0 % of the $^{1}H_\alpha$ and 93.1 % of the $^{13}C_\beta$ of residues 3–112. 81.6 % of side-chain protons were assigned as well. Figure 1c shows the difference in secondary chemical shifts $\Delta\delta(C_\alpha - C_\beta)$, sequential NOEs and DANGLE secondary structure predictions as a function of the primary structure for Miz 5–8. Positive and negative $\Delta\delta(C_\alpha - C_\beta)$ values are indicative of α-helices and β-strands, respectively. The number of secondary structure elements determined from the secondary chemical shifts indicates that the 4 ZFs adopt the consensus ββα fold, except for the first β strand of ZFs 7 and 8. $^{13}C_\alpha$ and $^{13}C_\beta$ chemical shifts of all cysteines

(except for those of Cys37 which could not be assigned) were consistent with the zinc-coordinating thiol state (Kornhaber et al. 2006). Likewise, the $^{13}C_{\delta 2}$ and $^{13}C_{\varepsilon 1}$ chemical shifts of all zinc-coordinating histidines (except that of His26, His 106 and His110 which could not be assigned) correlate with a zinc coordination mediated through the $N_{\varepsilon 2}$ (Barraud et al. 2012).

The ^{1}H–^{15}N HSQC spectrum of Miz 5–8 is displayed in Fig. 2a, b. Although the spectra show well-dispersed resonances, one can notice that most of the resonances from residues 27–44, which include the linker between ZFs 5 and 6 as well as the N-terminal region of ZF 6, are either weak or missing in the spectrum. This indicates that the backbone amide resonances are too weak (or broad) to be measured. This can be the result of conformational exchange on the µs–ms time-scale (R_{ex}), which broadens the resonances, and/or exchange between the $^{1}H_N$ and either the solvent deuterium or the suppressed protons from H_2O. The fact that our optimal folding conditions were found to be at a pH of 7 may contribute to the H_N exchange. Indeed, the intrinsic rate of amide exchange is faster at pH 7 than the minimal rates obtained around pH 4–5 (Bai et al. 1993; Eriksson et al. 1995).

Evidence of conformational exchange on the µs–ms timescale located in ZF 5 and 6

In order to further explore the causes for the vanishing amide resonances, we attempted amide exchange rate measurements. However, we found out it was not possible to resolubilize the lyophilized and folded Miz 5–8 construct to measure amide exchange rates. We have therefore resorted to the analysis of the pH dependence of the backbone amide resonance intensities on the ^{1}H–^{15}N HSQC. It is expected that the exchanging amide resonances will increase in intensity by decreasing the pH from 7.5 to 6.0, since the intrinsic rate of exchange slows down as the pH approaches a value of 4–5 (Bai et al. 1993; Eriksson et al. 1995).

We present in Fig. 3a, b the ^{1}H–^{15}N HSQCs of Miz 5–8 recorded at pH 7.5 and 6.0, respectively, and have labeled the resonances with pH-sensitive intensities. We also map these residues onto the backbone of an homology model of Miz 5–8 in a DNA-bound conformation generated using I-TASSER (Roy et al. 2010) (Fig. 3c, d). In addition, we have labeled in magenta the position of residues for which no resonances could be recorded on the ^{1}H–^{15}N HSQCs at any pH between 7.5 and 6.5. No significant changes in intensity were noted at pH lower than 6.5 and until pH 5.0 where a second set of resonances, most likely originating from the unfolded state (not shown), appeared. Only a few resonances shifted in the spectra between pH 7.5 and 6.5. Those belonged to histidine side-chains not involved in chelating the Zn^{2+} ions.

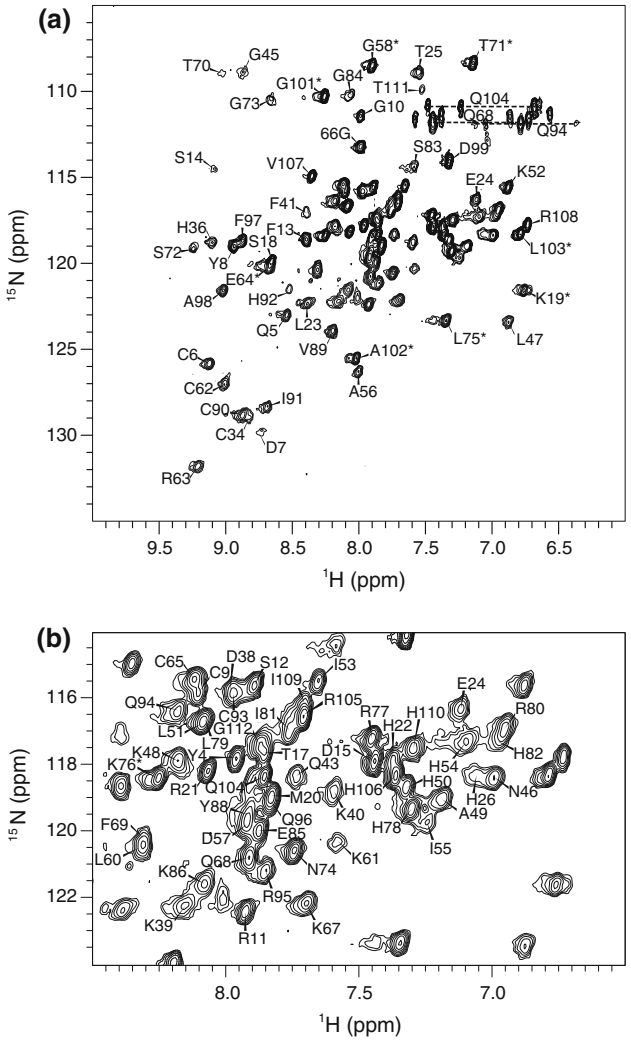

Fig. 2 ^{1}H–^{15}N HSQC spectrum of Miz 5–8 **a** Full ^{1}H–^{15}N HSQC spectrum of Miz 5–8 recorded at pH 7.0, 682 µM and 600 MHz. Resonances are labeled using the one-letter code. **b** Magnification of the crowded region of (**a**) for clarity. Resonances exhibiting processing-derived cardinal sinus wiggles have been labeled with an *asterisk*

One striking observation that can be made based on the results depicted in Fig. 3 is the fact that of the four helices, only the one in ZF 6 has pH-sensitive amides across its length as well as at the interface with the β-hairpin. Otherwise, and as expected due to end fraying effects, all four helices have pH-sensitive amides mainly located at their N- and C-termini. This indicates that the $^{1}H_N$ in the middle of the helix of ZF 6 are less protected from exchange with the solvent, and this result suggests a conformational exchange and/or opening of the tertiary structure involving the β-hairpin in this ZF. Additionally, the amide resonances of the unusual linker (DTDKE) between ZF 5 and 6, as well as those from the amides of His32, Lys33 and Cys37 located in the two β-strands are not observable in any HSQC recorded. This suggests that in

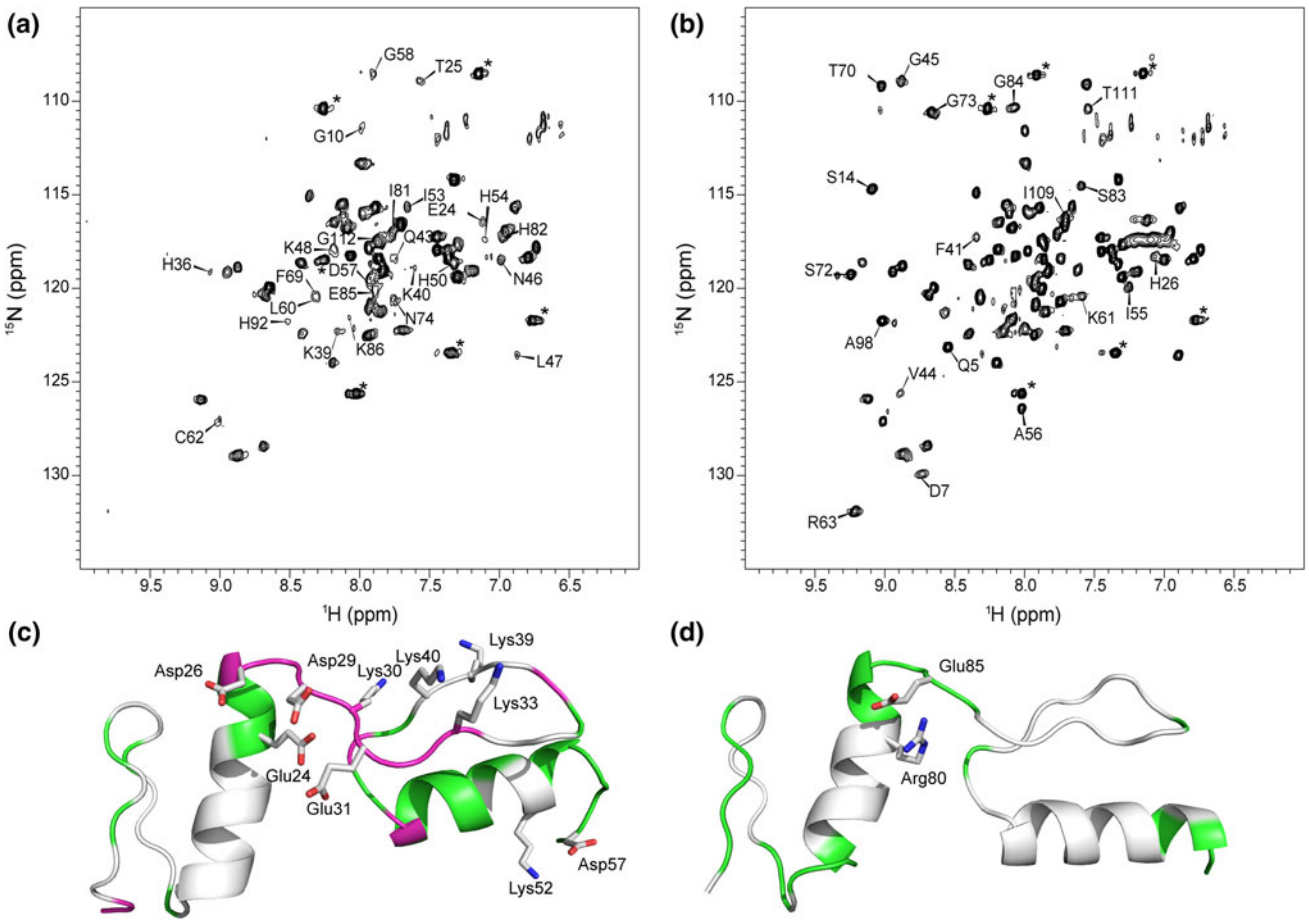

Fig. 3 Effect of pH on the intensities of Miz 5–8 backbone amide resonances. **a** ^{1}H–^{15}N HSQC spectrum of Miz 5–8 recorded at pH 7.5. Labeled resonances are those whose intensity increases when the pH is decreased. **b** ^{1}H–^{15}N HSQC spectrum of Miz 5–8 recorded at pH 6.0. Labeled resonances are those that have appeared between pH 7.5 and pH 6.0. Resonances exhibiting processing-derived cardinal sinus wiggles have been labeled with an *asterisk*. **c** and **d** depict homology models of ZFs 5–6 and ZFs 7–8, respectively. Resonances from residues broadened or weakened beyond detection are shown in *magenta* and the pH-sensitive residues are shown in *green*. Also shown are the side-chains of the acidic and basic clusters and those of the salt bridges involving the conserved basic and acidic side chains from the helices and the linkers. See text for details. The rendition was done with Pymol (www.pymol.org)

addition to amide exchange, the resonances of these amides may be broadened by conformational exchange (R_{ex}) occurring on the µs–ms timescale. In order to assess the presence of such a conformational exchange and characterize the presence of motions in the ps–ns and µs–ms timescales, we have employed ^{15}N-spin relaxation experiments.

^{15}N-spin relaxation

Heteronuclear NOEs ({^{1}H}–^{15}N NOE), ^{15}N–T_1 and ^{15}N–T_2 values recorded are presented on Fig. 4. In accordance with previous studies (Potter 2005; Zandarashvili et al. 2012), the {^{1}H}–^{15}N NOE measured in the strands and helices range between 0.6 and 0.8 and suggest limited librational movements of the backbone amides on the ps–ns timescale. In contrast, and as observed by the same groups, the backbone amides in the linkers between ZF 6 and 7 that could be measured display slightly lower values (approx. 0.4) and indicate movements with slightly larger amplitudes on the ns–ps timescale. However, these (positive) values clearly show that the inter-domain linkers are not completely disordered. Indeed, while the linkers between consecutive ZFs are more flexible than ZFs themselves, they remain somewhat rigid, resulting in the "quasi-ordered" conformation described by Potter (2005).

The average T_1 value recorded 620 ± 40 ms is very similar to 670 ± 67 ms, the average measured on a similar construct of 4 ZFs (Potter 2005). The average T_2 83 ± 21 ms recorded is also comparable but longer than those recorded for Miz 5–8 (i.e. 58 ± 6). As previously described by others (Brüschweiler et al. 1995; Potter 2005), the rotational diffusion of multi-ZF constructs is highly anisotropic. More precisely, ZFs located towards the center of multi-ZF

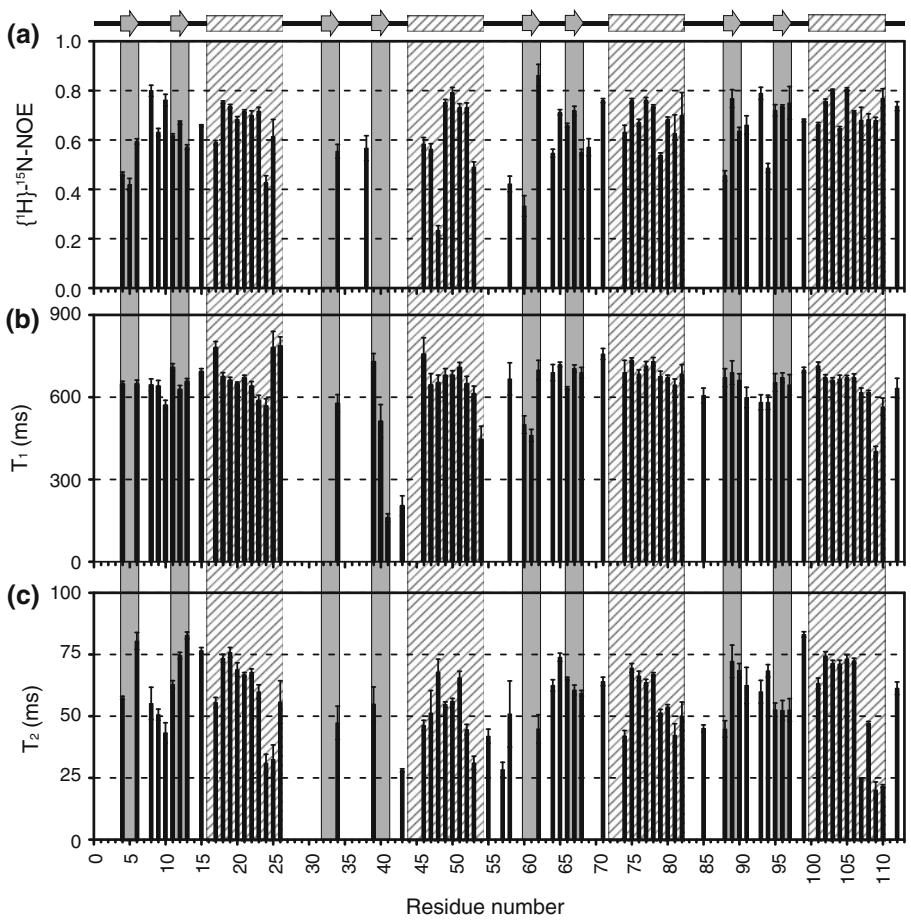

Fig. 4 ^{15}N relaxation measurements of the Miz 5–8 backbone amides on the ps–ns time-scale. **a** $\{^1H\}$–^{15}N–NOE, **b** T_1 and **c** T_2 values are plotted against the residue numbers. The β-strands and α-helices of the 4 ZFs are highlighted in *grey* and hatched, respectively

constructs experience anisotropic diffusion of higher intensity, with the N–H vectors of their α-helices aligned with the unique axis of the rotational diffusion tensor. This alignment contributes to decrease the effective correlation time experienced by rigid N–H vectors, which increases their T_1 and decreases their T_2 (Sauvé et al. 2004; Tjandra et al. 1997). However, elevated T_1/T_2 ratios are not always a sign of anisotropic rotational diffusion. Indeed, if a decrease in T_2 is not accompanied by an increase in T_1, there is a probability that the resulting elevated T_1/T_2 ratio is caused by conformational exchange (R_{ex}) occurring on the μs–ms time-scale. Inspection of Fig. 5a, b reveals that many of the residues with high T_1/T_2 ratios follow this trend and indicates the presence of such conformational exchange. In order to validate this postulation, we have carried out ^{15}N-relaxation dispersion or CPMG experiments at 600 MHz. Such experiments reduce the R_{ex} resonance broadening, and also allow estimation of the R_{ex} values (Ishima and Torchia 1999; Mittermaier and Kay 2009; Palmer 2004).

R_{ex} values are approximated by $R_{ex} \approx R_{2,eff}(\nu_{cpmg} \rightarrow 0) - R_{2,eff}(\nu_{cpmg} \rightarrow \infty)$, where ν_{cpmg} is the frequency of the refocusing 180° pulse. This frequency is given by $1/4\tau_{cpmg}$, with $2\tau_{cpmg}$ representing the time between successive refocusing pulses (see "Materials and methods" for further details). One convenient and rapid way to detect the presence of such conformational exchange is to compare HSQCs recorded with low and high CPMG refocusing rates. We present, in Fig. 6a, b HSQCs recorded at $\nu_{cpmg} = 33$ Hz and 1,000 Hz, respectively. Resonances undergoing conformational exchange gain in intensity upon the increase of the frequency of the refocusing pulses. Indeed, many low-intensity peaks at 33 Hz (broadened by R_{ex}) become more intense at 1,000 Hz. Moreover, some peaks broadened beyond detection at 33 Hz acquire intensities similar to the remaining resonances at high field strength. This clearly establishes the presence of μs–ms motions in the Miz 5–8 construct and a clear contribution of such motions to the shortening of many T_2 values.

Figure 5b displays the R_{ex} values estimated for residues that were not overlapped and for which a relaxation dispersion could be measured by fitting the $R_{2,eff}(\nu_{cpmg})$ curves as described in the materials and methods section. Shown in Fig. 5c are examples of such $R_{2,eff}(\nu_{cpmg})$ fits, and the associated fitted parameters are shown in supplementary material (Table S1). Interestingly, the R_{ex} values show a similar dependence on the sequence specific secondary structure as T_1/T_2 (Fig. 5a). Indeed, the largest R_{ex} values coincide with the largest T_1/T_2 ratios and are located

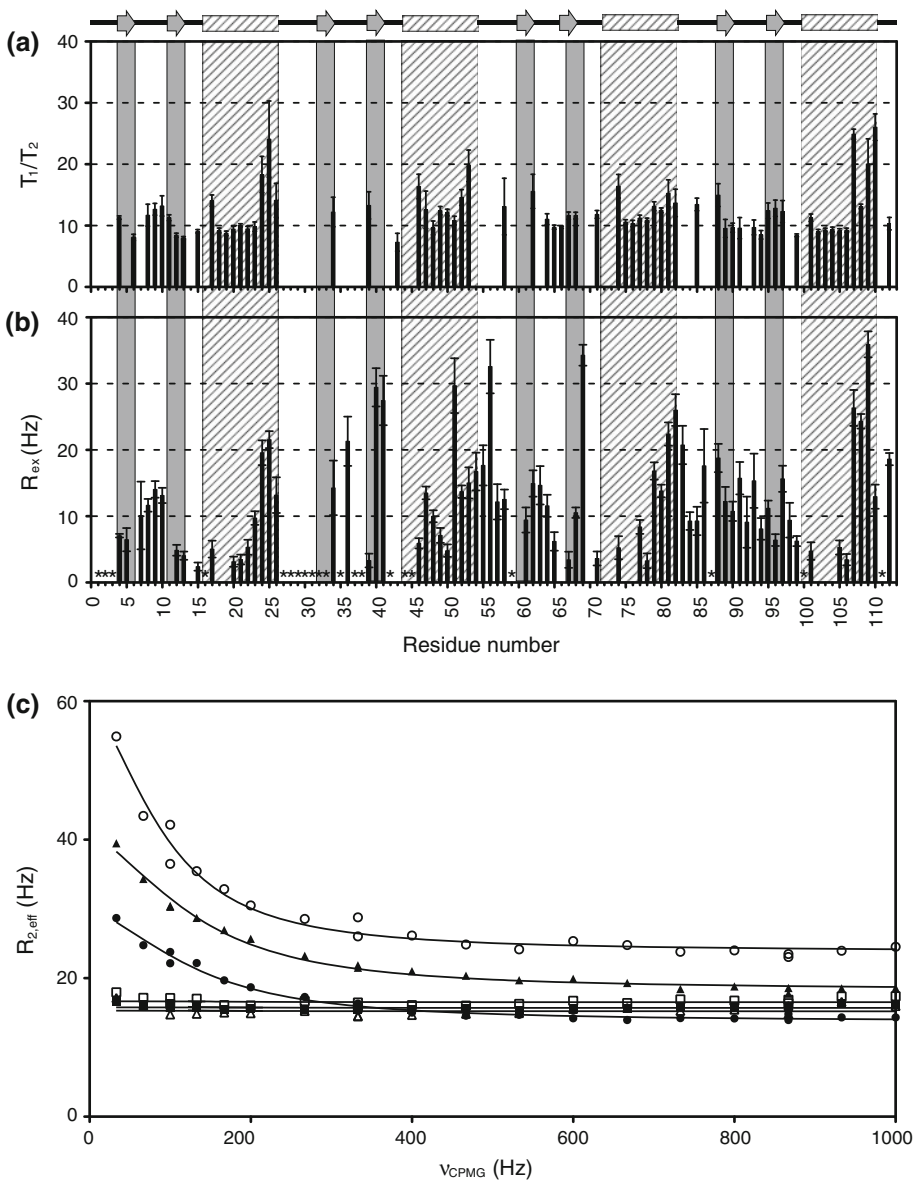

Fig. 5 T_1/T_2 and ^{15}N relaxation dispersion of Miz 5–8 backbone amides. **a** T_1/T_2 ratios and **b** R_{ex} plotted against the residue numbers The β-strands and α-helices of the 4 ZFs are highlighted in *grey* and hatched, respectively. *Asterisks* denote residues for which no dispersion could be measured due to extreme broadening of the resonances. Shown in (**c**) are representative ^{15}N relaxation dispersion profiles ($R_{2,eff}$ (ν_{CPMG})) for residues 9 (*filled circles*), 19 (*filled squares*), 24 (*filled triangles*), 40 (*open circles*), 75 (*open squares*) and 104 (*open triangles*). Note the absence of dispersion for residues 19, 75 and 104

near the end of the α-helices. To get a better appreciation of the phenomenon, we display the determined R_{ex} graphically on a ribbon representation of an homology model of Miz 5–8 in a DNA bound state (see Fig. 6c, d). The width of the ribbon is proportional to R_{ex}. As one can clearly notice, the largest R_{ex} values are located near the end of the helices and in the subsequent linkers, except for the linker between ZFs 7 and 8. On the other hand, it is interesting to note that the positions involved in DNA binding (towards the N-termini of the helices) do not undergo extensive μs–ms time-scale motions.

Solution structures of Miz-1 ZFs 5–7

The structure of ZF 8 has already been solved by our group (Bédard et al. 2012) as part of the Miz 8–10 construct (PDB identification code 2LVR). Hence, we will focus on the description of the solution structures of ZFs 5–7. The restraints used to calculate the structure of each ZF (NOEs, dihedral angles and H-bond restraints) are summarized in Table 1. The structures of ZFs 5–7 are shown in Fig. 7. As can be seen, the selected structures for ZFs 5 and 7 display excellent convergence, with RMSD values of 0.3 ± 0.1 Å and 0.26 ± 0.06 Å, respectively, for the backbone atoms (C_α, C', O, N) of the consensus ZF sequences. In both ZFs, all conserved side chains (hydrophobic or zinc-coordinating) are also well defined by the set of restraints used. As observed for the solution structures reported earlier, the hairpin between the two β strands as well as the region between the second β strand and the α helix on both ZFs are not quite as well defined, due to a lack of observable NOEs (see supplementary figure 1). The N- and C-terminus of the

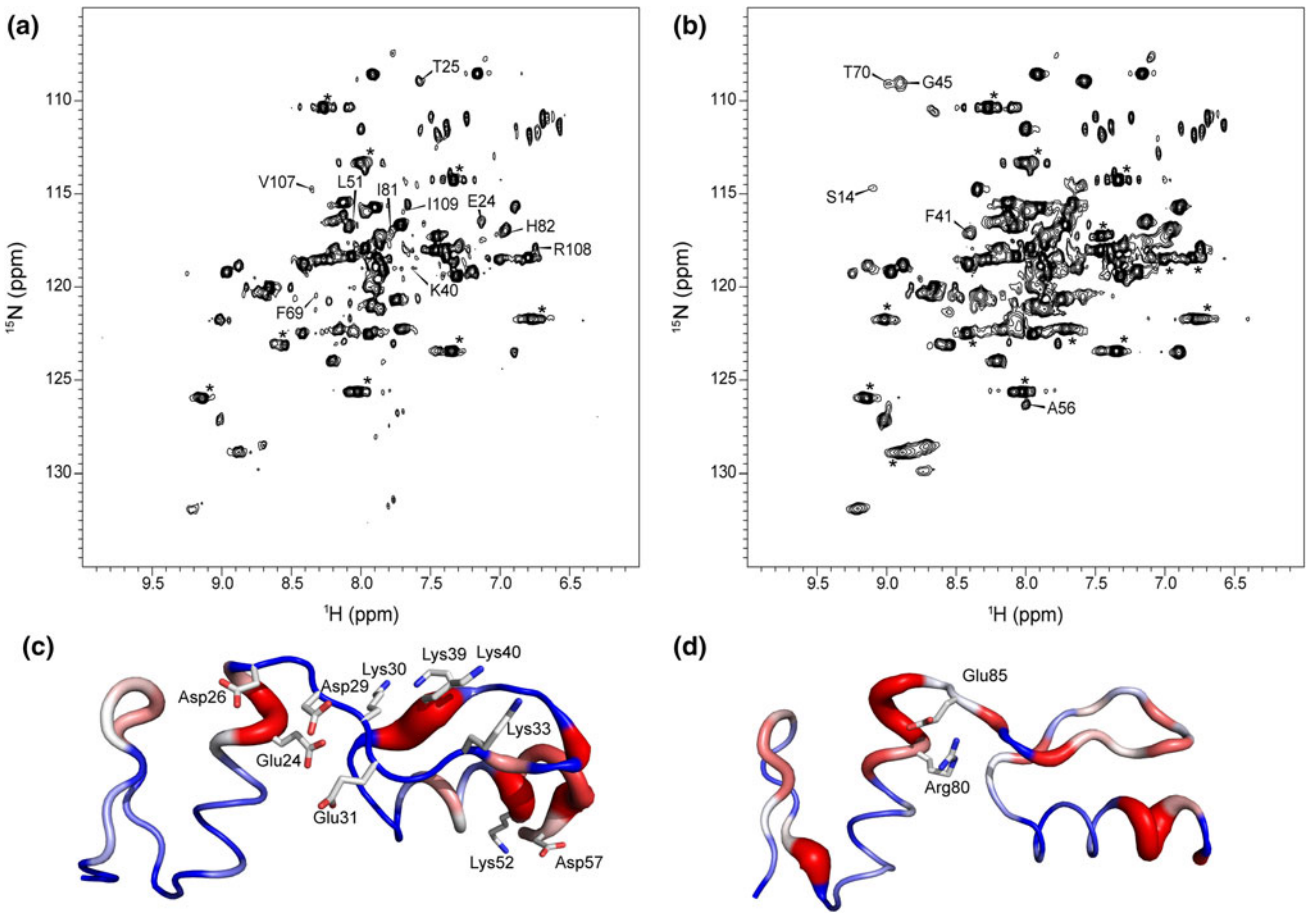

Fig. 6 ^{15}N relaxation dispersion of Miz 5–8 backbone amides. HSQC spectra recorded with a CPMG frequency of 33 Hz (**a**) and 1,000 Hz (**b**), respectively. Labeled resonances in (**a**) exhibit a large increase of intensity (**a**) or appear (**b**) as the CPMG frequency is increased. Resonances exhibiting processing-derived cardinal sinus wiggles have been labeled with an *asterisk*. **c** and **d** depict homology models of ZFs 5–6 and ZFs 7–8, respectively. The width of the backbone worm is proportional to the R_{ex} displayed in Fig. 4c. Note the color-coding: residues in *blue* have low R_{ex} while residues in *red* have large R_{ex} values. Also shown are the side-chains of the acidic and basic clusters and those of the salt-bridges involving the conserved basic and acidic side-chains from the helices and the linkers. See text for details. The rendition were done with Pymol (www.pymol.org)

consensus sequence of ZF 5 and 7 are not as well defined as the remainder of the core residues (Fig. 8).

The α helix of ZF 6 is well folded, with a RMSD value of 0.23 ± 0.06 Å for the backbone of helical residues (residues 45–55). The RMSD values for the backbone of helical residues of ZFs 5 and 7 are 0.17 ± 0.07 Å and 0.13 ± 0.04 Å, respectively (residues 16–27 for ZF 5 and residues 72–83 for ZF 7). In comparison, the backbone RMSD value of ZF 6 consensus sequence (residues 32–54) is 0.95 ± 0.26 Å, which is triple that of the other ZFs.

Resonances for amino acids 1–2 and 27–33 in ZF 5 and 6 could not be observed in any spectrum. Partly because of this, too few long-range and tertiary NOEs could be unambiguously assigned in ZF 6 (see Table 1) to define the expected ββα fold, despite the aforementioned DANGLE predictions. This lack of NOEs and resonance absence is most likely caused by the exchange broadening and/or rapid amide exchange discussed above at pH 7.0.

Discussion and conclusion

Miz-1 is a BTB/POZ transcription factor that contains 13 C_2H_2 ZFs that activates the transcription of cell cycle inhibitors (e.g. $p15^{INK4b}$ and $p21^{CIP1}$). Although DNA binding and protein–protein interactions (e.g. with SMAD3) involving the ZFs are important for transcriptional activation, it is not known how these ZFs bind the promoters of activated genes and how they bind to SMAD3/4. In order to provide structural information on these fundamental issues, we report the structural and dynamical characterization by solution-state NMR spectroscopy of a Miz-1 construct composed of residues 416–526, which encompasses ZF 5–8.

Whereas ZFs 5, 7 and 8 adopt a canonical and stable ββα fold at neutral pH, the NMR data collected under these conditions indicate that ZF 6 and the linker between ZFs 5 and 6 are undergoing conformational exchange. Upon

Table 1 Structural statistics for ZFs 5–7 of Miz-1

	ZF 5	ZF 6	ZF 7
Restraints for final structure calculations			
NOE distance restraints			
Intraresidue ($\|i - j\| = 0$)	287	219	391
Sequential ($\|i - j\| = 1$)	128	94	163
Medium range ($1 < \|i - j\| < 5$)	101	77	118
Long range ($\|i - j\| \geq 5$)	66	10	113
Total NOE distance restraints	582	400	785
Hydrogen bonds	12 × 2	7 × 2	13 × 2
Zinc ligands	4 × 2	4 × 2	4 × 2
Dihedral angle restraints[a]			
ϕ and ψ angles	49	51	49
χ angles	3	1	4
Structure statistics (20 structures)			
Number of NOE violations >0.5 Å	0	0	0
Number of dihedral angle violations >5 °	0	0	0
RMS deviations from experimental data			
Average distance restraint violation (Å)	0.035 ± 0.006	0.009 ± 0.002	0.029 ± 0.004
Average dihedral restraint violation (°)	0.3 ± 0.1	0.5 ± 0.2	0.8 ± 0.1
RMS deviation to mean coordinates			
Backbone heavy atoms (Å)	1.7 ± 0.5	1.9 ± 0.6	0.7 ± 0.2
All heavy atoms (Å)	2.3 ± 0.5	2.5 ± 0.6	1.4 ± 0.3
For ZF consensus sequences[b]			
Backbone heavy atoms (Å)	0.3 ± 0.1	1.0 ± 0.3	0.26 ± 0.06
All heavy atoms (Å)	1.0 ± 0.1	2.0 ± 0.5	1.0 ± 0.1
α-helical residues[c]			
Backbone heavy atoms (Å)	0.17 ± 0.07	0.23 ± 0.06	0.13 ± 0.04
All heavy atoms (Å)	1.0 ± 0.2	0.9 ± 0.1	0.9 ± 0.2
Ramanchandran plot statistics[d] (%)			
Residues in most favored regions	95.0	88.3	91.4
Residues in additionally allowed regions	5.0	11.1	8.6
Residues in generously allowed regions	0.0	0.6	0.0
Residues in disallowed regions	0.0	0.0	0.0

[a] ϕ and ψ angles were derived from the program DANGLE

[b] ZF consensus sequences comprise residues 4–26 for ZF 5, 32–54 for ZF 6 and 60–82 for ZF 7

[c] α-helical residues comprise residues 16–27 for ZF5, 45–55 for ZF6 and 72–83 for ZF7

[d] Ramanchandran plot statistics were generated using PROCHECK_NMR for ZF consensus sequences

inspection of the primary structure of Miz 5–8 (Fig. 1a), many unusual features can be recognized. One of them is the presence of a histidine instead of the conserved aromatic residues Phe and Tyr (Schmidt 2004), two positions before the first zinc-coordinating cysteine of ZF 6. Upon inspection of other ZF solution structures found on the PDB (such as 1VA1 or 2DMD), one can notice that a histidine in this position can cause local conformational fluctuations.

Secondly, and most strikingly, the sequence of the linker between ZF 5 and ZF 6 (DTDKE) is highly uncharacteristic. Indeed, compared to the consensus TGEKP, only the lysine is conserved. Moreover, the sequence contains three negatively charged side chains. In addition, the glutamate (Glu24) found two residues before the last histidine in ZF 5 is also highly unusual. Indeed, arginine (62.2 %), lysine (12.4 %) or a hydrophobic amino acid (16.9 %) are the usual amino acids found at this position in a database consisting of 2,435 human ZFs (Schmidt 2004). The importance of a salt bridge between the conserved basic side chain and the conserved glutamate in the TG**E**KP linker has recently been demonstrated for inter-ZF movements in the three ZFs of Egr-1 (Zandarashvili et al. 2012). In fact, in the WT primary

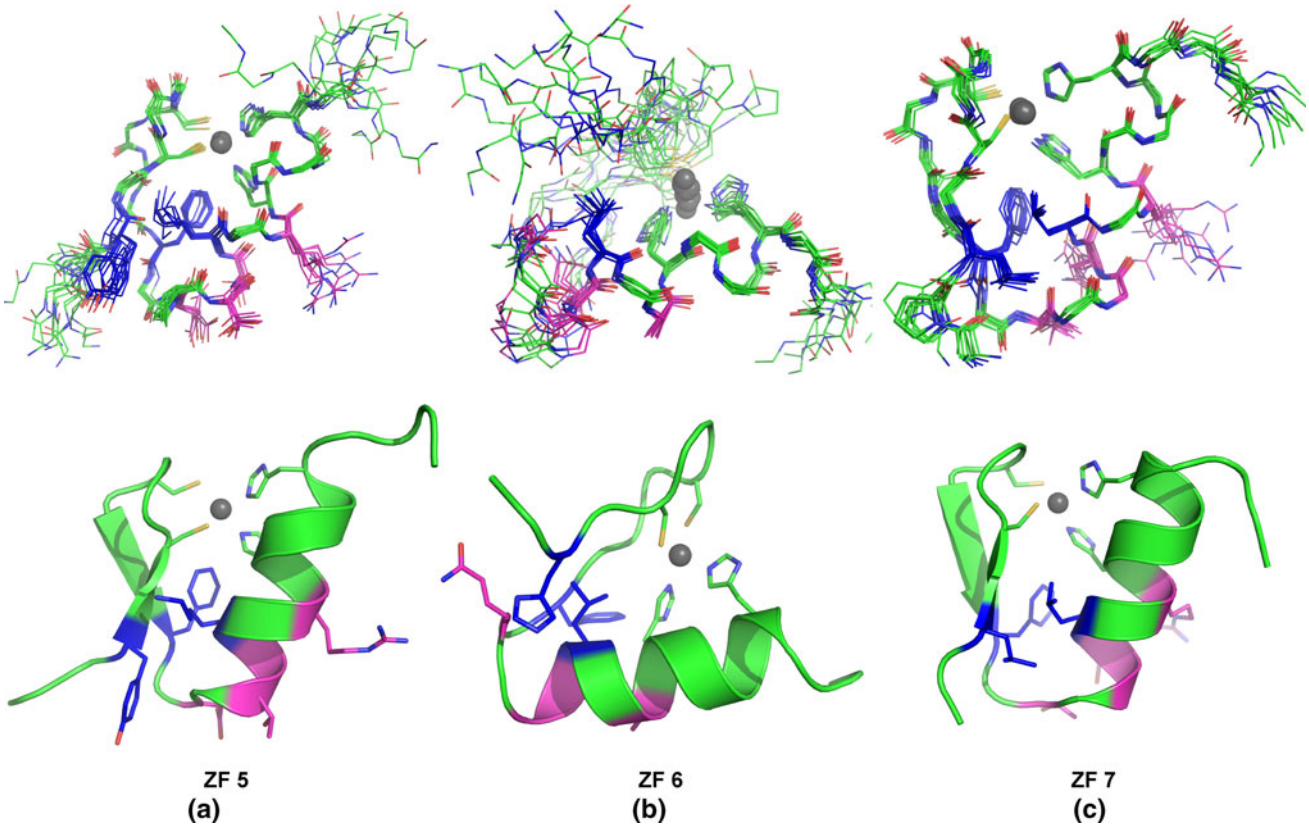

Fig. 7 NMR solution structures of (**a**) ZF 5, (**b**) ZF 6 and (**c**) ZF 7. The backbone atoms, as well as the side chains of zinc-coordinating (carbon atoms in *green*), hydrophobic core residues (carbon atoms in *blue*) and residues that would putatively contact DNA (carbon atoms in *magenta*) are depicted. The Zn^{2+} ions are shown as *grey balls*. All three structures are a superposition of the 10 lowest energy structures. The rendition and superposition were done with Pymol (www.pymol.org)

structure of Egr-1, the basic side chain and the glutamate are replaced by a threonine in ZF 1 and a glutamine in the linker, respectively. The engineering of a salt bridge between a lysine and a glutamate in the TG**E**KP linker was shown to reduce movements experienced by ZF 1 in absence of DNA. As argued by Zandarashvili et al. (2012), the presence of such movements in the WT constructs plays a key role in the search process for the specific DNA sequence of Egr-1. But while Egr-1's threonine-glutamine pair merely lacks the stabilizing salt bridge, the equivalent residues between Miz 5–8's ZFs 5 and 6 (Glu24 and Asp29) are both negatively charged residues, which are mutually repulsive. Assuming that the Miz 5–8 construct can adopt a classical DNA-bound state, we have generated a homology model of such a conformation (Fig. 3c). In this conformation, the side chains of Asp27 and Glu31 are also oriented towards Glu24 and Asp29, which should further destabilize this region of the protein. It is also important to note that in a DNA complex, this negatively charged cluster would be situated close to the phosphodiester backbone. This canonical conformation for the linker between ZF 5 and 6 is therefore expected to be highly unfavorable for DNA binding.

Another destabilizing cluster, formed by Lys30, Lys33, Lys39 and Lys40, is situated in the putative β-sheet of ZF 6. Thus, with these two charged clusters, it is expected that the free energy of the state where ZFs 5 and 6 adopt a classical DNA-bound conformation would be elevated. This results in the low probability of adoption of this conformation by these two ZFs. We propose that this could contribute to the local destabilization of the tertiary structure of ZF 6 and explain the extreme broadening of resonances observed in this region of the construct, as well as the lack of long-range and tertiary NOEs.

ZFs 1–4 have been shown to interact with MH1 domain of SMAD3/4. Indeed, examination of the primary sequence of those ZFs reveals a high amount of hydrophobic side chains in lieu of the expected polar side chains in the residues expected recognize DNA (positions—1, 2, 3 and 6 of the ZF α-helix), supporting their participation in protein–protein interactions. Knowing that ZF 6 undergoes conformational exchange and possesses unusual charged residues in its sequence that could prevent it from binding DNA, we hypothesize that ZF 6 could play a hinge-like role, separating a protein–protein interaction domain from a DNA-interacting domain. This

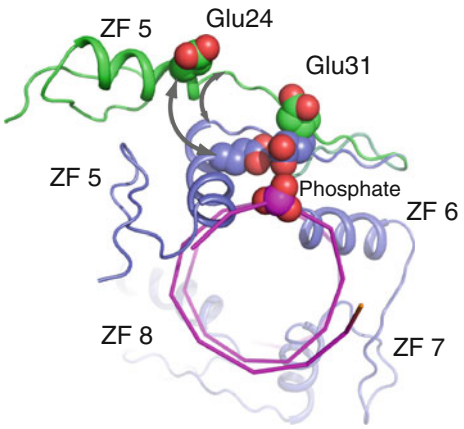

Fig. 8 Molecular model for the conformational exchange located in ZFs 5 and 6. This model displays the putative hinge function of these ZFs in the structural biology of Miz-1. As described in the text, in a canonical DNA complex, electrostatic repulsions between negatively charged side chains (e.g. Glu24 and Glu31) and phosphates (Glu31) can be predicted to occur. Note that many intra-molecular repulsions are also expected to be present (see Fig. 6) in a DNA-binding competent configuration of ZFs 5 and 6. We propose that these enthalpically unfavorable states (*blue ribbon* and carbon atoms) will promote local conformational fluctuations that would bring ZF 5 on and off DNA (*magenta strings*). The local unfolding of the last helical turn of ZF 5 and transient opening of the tertiary structure between the first strand and the helix of ZF 6 (*green ribbon* and carbon atoms) are logical possible fluctuations according to our results. As described in the text and on Fig. 7, the presence of a His (instead of the more conserved Tyr and Phe) could contribute to such a movement. The rendition and superposition were done with Pymol (www.pymol.org)

peculiar sequence and resultant dynamical behavior could be important for Miz-1 function by promoting the availability of ZF 1–4 to engage protein–protein interaction with SMAD3/4, and potentially other protein–protein interactions involving ZFs 1–5.

Interestingly, Zandarashvili et al. have also reported the presence of ^{15}N-R_{ex} located at the end of the helix of ZF 1, the first linker and the β-hairpin of the next ZF (Zandarashvili et al. 2012). In addition, residues with significant ^{15}N-R_{ex} were located at the end of the helix in ZF 2. As one can notice in Fig. 5, T_1/T_2 ratios are on average higher in helices than in β-sheets, and that they increase strikingly as they approach the C-terminus of the helices. This trend has also been found in all the ZFs of the Miz 8–10 construct (data not shown), as well as in many other poly-ZF proteins (Brüschweiler et al. 1995; Potter 2005; Zandarashvili et al. 2012). To date, this information has been attributed to anisotropy and results obtained by the model-free analysis have suggested that the helices aligned with the unique axis of their poly-ZFs constructs (Brüschweiler et al. 1995; Potter 2005). In light of our results, we propose that this rise in T_1/T_2 ratios at the C-terminus of helices could be attributed to the concerted effects of rotational diffusion anisotropy and R_{ex}. As can be seen on Fig. 5, high values of R_{ex} are found in numerous positions in the Miz 5–8 construct, and strikingly coincide with high T_1/T_2 ratios in α-helices.

Acknowledgments This work was supported by the Natural Science and Engineering Research Council (NSERC) of Canada (grant to P.L. and studentships to M.B. and D.B.) and by the Regroupement stratégique sur la fonction, la structure et l'ingénierie des protéines (PROTEO). D.B. also acknowledges PROTEO for the award of graduate studentship. The authors thank Dr. Frank Hänel (Hans-Knöll-Institut für Naturstoff-Forschung e.V, Germany) for kindly providing us with the Miz-1 cDNA, Dr. Yves L. Dory (Université de Sherbrooke, Canada) for giving access and advice to use his HPLC system, Dr. Jean-François Naud for the initial cloning and Dr. Martin Montagne for his helpful comments on the manuscript. Finally, we thank Prof. Jim Omichinski (U. de Montréal) for his help with the refolding protocol of Zinc Fingers.

References

Bai Y, Milne JS, Mayne L, Englander SW (1993) Primary structure effects on peptide group hydrogen exchange. Proteins 17:75–86. doi:10.1002/prot.340170110

Barraud P, Schubert M, Allain FH-T (2012) A strong 13C chemical shift signature provides the coordination mode of histidines in zinc-binding proteins. J Biomol NMR 53:93–101. doi:10.1007/s10858-012-9625-6

Bédard M, Maltais L, Beaulieu M-E et al (2012) NMR structure note: solution structure of human Miz-1 zinc fingers 8–10. J Biomol NMR. doi:10.1007/s10858-012-9670-1

Berg JM (1988) Proposed structure for the zinc-binding domains from transcription factor IIIA and related proteins. Proc Natl Acad Sci USA 85:99–102

Bowen H (2003) Characterization of the Murine Nramp1 promoter: requirements for transactivation by Miz-1. J Biol Chem 278:36017–36026. doi:10.1074/jbc.M304301200

Brayer KJ, Segal DJ (2008) Keep your fingers off my DNA: protein–protein interactions mediated by C_2H_2 zinc finger domains. Cell Biochem Biophys 50:111–131. doi:10.1007/s12013-008-9008-5

Brünger AT, Adams PD, Clore GM et al (1998) Crystallography & NMR system: a new software suite for macromolecular structure determination. Acta Crystallogr D Biol Crystallogr 54:905–921

Brüschweiler R, Liao X, Wright PE (1995) Long-range motional restrictions in a multidomain zinc-finger protein from anisotropic tumbling. Science 268:886–889

Delaglio F, Grzesiek S, Vuister GW et al (1995) NMRPipe: a multidimensional spectral processing system based on UNIX pipes. J Biomol NMR 6:277–293

Emerson RO, Thomas JH (2009) Adaptive evolution in zinc finger transcription factors. PLoS Genet 5:e1000325. doi:10.1371/journal.pgen.1000325

Eriksson MA, Härd T, Nilsson L (1995) On the pH dependence of amide proton exchange rates in proteins. Biophys J 69:329–339. doi:10.1016/S0006-3495(95)79905-2

Farrow NA, Muhandiram R, Singer AU et al (1994) Backbone dynamics of a free and phosphopeptide-complexed Src homology 2 domain studied by 15N NMR relaxation. Biochemistry 33:5984–6003

Hyre DE, Klevit RE (1998) A disorder-to-order transition coupled to DNA binding in the essential zinc-finger DNA-binding domain of yeast ADR1. J Mol Biol 279:929–943. doi:10.1006/jmbi.1998.1811

Ishima R, Torchia DA (1999) Estimating the time scale of chemical exchange of proteins from measurements of transverse relaxation rates in solution. J Biomol NMR 14:369–372

Kornhaber GJ, Snyder D, Moseley HNB, Montelione GT (2006) Identification of zinc-ligated cysteine residues based on 13Cα and 13Cβ chemical shift data. J Biomol NMR 34:259–269. doi:10.1007/s10858-006-0027-5

Laskowski RA, Rullmannn JA, MacArthur MW et al (1996) AQUA and PROCHECK-NMR: programs for checking the quality of protein structures solved by NMR. J Biomol NMR 8:477–486

Lipchock J, Loria JP (2009) Millisecond dynamics in the allosteric enzyme imidazole glycerol phosphate synthase (IGPS) from Thermotoga maritima. J Biomol NMR 45:73–84. doi:10.1007/s10858-009-9337-8

Luz Z, Meiboom S (1963) Nuclear magnetic resonance study of the protolysis of trimethylammonium ion in aqueous solution—order of the reaction with respect to solvent. J Chem Phys 39:366–370. doi:10.1063/1.1734254

Mittermaier AK, Kay LE (2009) Observing biological dynamics at atomic resolution using NMR. Trends Biochem Sci 34:601–611. doi:10.1016/j.tibs.2009.07.004

Mulder FA, Mittermaier A, Hon B et al (2001a) Studying excited states of proteins by NMR spectroscopy. Nat Struct Biol 8:932–935. doi:10.1038/nsb1101-932

Mulder FA, Skrynnikov NR, Hon B et al (2001b) Measurement of slow (micros-ms) time scale dynamics in protein side chains by (15)N relaxation dispersion NMR spectroscopy: application to Asn and Gln residues in a cavity mutant of T4 lysozyme. J Am Chem Soc 123:967–975

Palmer AG (2004) NMR characterization of the dynamics of biomacromolecules. Chem Rev 104:3623–3640. doi:10.1021/cr030413t

Palmer AG, Kroenke CD, Loria JP (2001) Nuclear magnetic resonance methods for quantifying microsecond-to-millisecond motions in biological macromolecules. Methods Enzymol 339:204–238

Peukert K, Staller P, Schneider A et al (1997) An alternative pathway for gene regulation by Myc. EMBO J 16:5672–5686. doi:10.1093/emboj/16.18.5672

Potter BM (2005) The six zinc fingers of metal-responsive element binding transcription factor-1 form stable and quasi-ordered structures with relatively small differences in zinc affinities. J Biol Chem 280:28529–28540. doi:10.1074/jbc.M505217200

Razin SV, Borunova VV, Maksimenko OG, Kantidze OL (2012) Cys2His2 zinc finger protein family: classification, functions, and major members. Biochem Mosc 77:217–226. doi:10.1134/S0006297912030017

Rieping W, Habeck M, Bardiaux B et al (2007) ARIA2: automated NOE assignment and data integration in NMR structure calculation. Bioinformatics 23:381–382. doi:10.1093/bioinformatics/btl589

Roy A, Kucukural A, Zhang Y (2010) I-TASSER: a unified platform for automated protein structure and function prediction. Nat Protoc 5:725–738. doi:10.1038/nprot.2010.5

Sauvé S, Tremblay L, Lavigne P (2004) The NMR solution structure of a mutant of the Max b/HLH/LZ free of DNA: insights into the specific and reversible DNA binding mechanism of dimeric transcription factors. J Mol Biol 342:813–832. doi:10.1016/j.jmb.2004.07.058

Schmidt D (2004) Adaptive evolution drives the diversification of zinc-finger binding domains. Mol Biol Evol 21:2326–2339. doi:10.1093/molbev/msh246

Seoane J, Pouponnot C, Staller P et al (2001) TGFbeta influences Myc, Miz-1 and Smad to control the CDK inhibitor p15INK4b. Nat Cell Biol 3:400–408. doi:10.1038/35070086

Seoane J, Le H-V, Massagué J (2002) Myc suppression of the p21(Cip1) Cdk inhibitor influences the outcome of the p53 response to DNA damage. Nature 419:729–734. doi:10.1038/nature01119

Staller P, Peukert K, Kiermaier A et al (2001) Repression of p15INK4b expression by Myc through association with Miz-1. Nat Cell Biol 3:392–399. doi:10.1038/35070076

Stead MA, Trinh CH, Garnett JA et al (2007) A beta-sheet interaction interface directs the tetramerisation of the Miz-1 POZ domain. J Mol Biol 373:820–826. doi:10.1016/j.jmb.2007.08.026

Stogios PJ, Cuesta-Seijo JA, Chen L et al (2010) Insights into strand exchange in BTB domain dimers from the crystal structures of FAZF and Miz1. J Mol Biol 400:983–997. doi:10.1016/j.jmb.2010.05.028

Tjandra N, Garrett DS, Gronenborn AM et al (1997) Defining long range order in NMR structure determination from the dependence of heteronuclear relaxation times on rotational diffusion anisotropy. Nat Struct Biol 4:443–449

Vranken WF, Boucher W, Stevens TJ et al (2005) The CCPN data model for NMR spectroscopy: development of a software pipeline. Proteins 59:687–696. doi:10.1002/prot.20449

Wang C, Grey MJ, Palmer AG (2001) CPMG sequences with enhanced sensitivity to chemical exchange. J Biomol NMR 21:361–366

Wanzel M, Russ AC, Kleine-Kohlbrecher D et al (2008) A ribosomal protein L23-nucleophosmin circuit coordinates Miz1 function with cell growth. Nat Cell Biol. doi:10.1038/ncb1764

Wishart DS, Bigam CG, Yao J et al (1995) 1H, 13C and 15N chemical shift referencing in biomolecular NMR. J Biomol NMR 6:135–140

Wolfe SA, Nekludova L, Pabo CO (2000) DNA recognition by Cys2His2 zinc finger proteins. Annu Rev Biophys Biomol Struct 29:183–212. doi:10.1146/annurev.biophys.29.1.183

Zandarashvili L, Vuzman D, Esadze A et al (2012) Asymmetrical roles of zinc fingers in dynamic DNA-scanning process by the inducible transcription factor Egr-1. Proc Natl Acad Sci. doi:10.1073/pnas.1121500109